ADVANCED MATERIALS

www.advmat.de

The Functional Response of Mesenchymal Stem Cells to Electron-Beam Patterned Elastomeric Surfaces Presenting Micrometer to Nanoscale Heterogeneous Rigidity

Manus J. P. Biggs, Marc Fernandez, Dilip Thomas, Ryan Cooper, Matteo Palma, Jinyu Liao, Teresa Fazio, Carl Dahlberg, Helen Wheadon, Anuradha Pallipurath, Abhay Pandit, Jeffrey Kysar, and Shalom J. Wind**

Cells directly probe and respond to the physicomechanical properties of their extracellular environment, a dynamic process which has been shown to play a key role in regulating both cellular adhesive processes and differential cellular function. Recent studies indicate that stem cells show lineage-specific differentiation when cultured on substrates approximating the stiffness profiles of specific tissues. Although tissues are associated with a range of Young's modulus values for bulk rigidity, at the subcellular level, tissues are comprised of heterogeneous distributions of rigidity. Lithographic processes have been widely explored in cell biology for the generation of analytical substrates to probe cellular physicomechanical responses. In this work, it is shown for the first time that that direct-write e-beam exposure can significantly alter the rigidity of elastomeric poly(dimethylsiloxane) substrates and a new class of 2D elastomeric substrates with controlled patterned rigidity ranging from the micrometer to the nanoscale is described. The mechanoresponse of human mesenchymal stem cells to e-beam patterned substrates was subsequently probed in vitro and significant modulation of focal adhesion formation and osteochondral lineage commitment was observed as a function of both feature diameter and rigidity, establishing the groundwork for a new generation of biomimetic material interfaces.

Cells directly probe and respond to the physicomechanical properties of their extracellular environment through adhesion complexes and tractive-mediated matrix deformation.[1] Increasingly, it is evident that matrix or tissue elasticity has a key role in regulating multiple cell processes,[2] including adhesion,[3] migration,[4,5] and differential function[6,7] through cell-generated actomyosin interactive forces regulated by cell–substrate adhesion and dynamic feedback mechanisms.[5]

The sensitivity of cells to the mechanical properties of the extracellular matrix (ECM) is attributable to the mechanosensitive nature of the proteins associated with cell–ECM supramolecular adhesive complexes.[8] Among these adhesive structures, focal adhesions (FAs) appear to be the most critical, as shown by the reported correlation between FA size to a sustained force exhibiting a constant stress.[9,10] This mechanosensitivity is thought to be

Dr. M. J. P. Biggs, M. Fernandez, D. Thomas, Prof. A. Pandit
Centre for Research in Medical Devices (CÚRAM)
Biosciences Research Building
National University of Ireland
Newcastle Road, Dangan, Galway, Ireland
E-mail: manus.biggs@nuigalway.ie

Dr. M. J. P. Biggs, M. Fernandez, Prof. A. Pandit
Department of Biomedical Engineering
College of Engineering and Informatics
National University of Ireland Galway
Galway, Ireland

Dr. R. Cooper, Dr. C. Dahlberg, Prof. J. Kysar
Department of Mechanical Engineering
Columbia University
500 West 120th St, New York, NY 10027, USA

Dr. M. Palma
The School of Biological and Chemical Sciences
Queen Mary University of London
London E1 4NS, UK

J. Liao
Department of Electrical Engineering
Columbia University
500 West 120th St, New York, NY 10027, USA

Dr. J. Liao, Dr. T. Fazio, Prof. S. J. Wind
Department of Applied Physics and Applied Mathematics
Columbia University
500 West 120th St, New York, NY 10027, USA
E-mail: sw2128@columbia.edu

Dr. H. Wheadon
Paul O'Gorman Leukaemia Research Centre
The University of Glasgow
Glasgow G11 0YN, UK

Dr. A. Pallipurath
Department of Chemistry
University of Bath
Claverton Down, Bath BA2 1AG, UK

DOI: 10.1002/adma.201702119

regulated by a conserved local mechanism in which subcellular forces induce an elastic deformation of transmembrane integrin regions, triggering conformational and organizational changes, resulting in integrin activation and subsequent exposure of cryptic binding sites enabling FA reinforcement.[11] These interactive processes should set a dimensional scale for cellular rigidity sensing.

Modulation to FA formation has been implicated in the onset of differential cell function[12] and recent studies indicate that stem cells show lineage-specific differentiation when cultured in vitro on substrates matching the bulk stiffness corresponding to specific tissues. Although tissues are associated with a broad range of Young's modulus values for bulk rigidity, at the subcellular level, and particularly at the micro- and nanoscales, tissues are composed of heterogeneous distributions of cellular elements, extracellular particles, and fibers of varying mechanical properties. Specifically, skeletal stem cells reside in a specialized biophysical and biochemical niche environment which is thought to present physicomechanical cues critical to phenotype maintenance and in preventing the loss of cell stemness.[12] ECM architectures encountered by skeletal stem cells in vivo range from the microscale (insoluble fibrillar ECM proteins), to the nanoscale (mineral crystals), with elastic moduli ranging from 2–7 kPa (plasma membrane)[13] to 5 GPa (collagen type I)[14] to 150 GPa (hydroxyapatite).[15] Critically, how cells sense and respond to the mechanical properties of their surroundings in a heterogeneous environment and the role of mechanical heterogeneity in mediating skeletal stem cell function remains poorly understood.[4,16]

Elastomeric substrates and hydrogels have been used to present cells with surfaces of specific stiffness, approximating the range of rigidities encountered in physiological environments.[7] Critically, substrates possessing bulk rigidity of ≈20–50 kPa have been previously shown to induce stem cell differentiation to cartilage and bone-specific lineages in vitro.[7,17] Poly(dimethylsiloxane) (PDMS), in particular, has recently found widespread use in cell adhesion/migration assays[18] microfluidic and MEMS technologies[19] due to its favorable optical, biocompatibility, and mechanical properties. Indeed, PDMS substrates have been used to study the role of extracellular rigidity on cellular adhesion[20] and differentiation,[21] due to the ease by which its rigidity may be precisely controlled by simply varying the base:accelerator formulation ratio.

Within the realms of micro and nanofabrication, lithographic-derived processes have been widely explored in cell biology for the generation of analytical substrates for probing physicochemical responses at the cellular and subcellular level. In particular, PDMS has been immensely useful for nanoscale patterning of proteins (soft lithography, microcontact printing) and for the generation of pillar substrates with differential rigidity to probe cell-generated extracellular forces.[9] Significantly, unlike traditional photo-crosslinkable materials and photoresists, PDMS is transparent in the visible and ultraviolet wavelengths and cannot, in general, be directly patterned by standard photolithography,[22] without the addition of a photoactive compound.[23] However, PDMS has been shown to be sensitive to deep-UV and e-beam irradiation,[23–25] which induces cross-linking of the elastomer.

In this work, we show that direct e-beam exposure can significantly alter the rigidity of PDMS. This has enabled us to develop a new class of 2D elastomeric substrates with geometrically patterned regions of heterogeneous rigidity. Specifically, we studied the mechanoresponse of human skeletal stem cells (hMSCs) cultured on ≈35 kPa elastomer substrates, modified to present surface patterns of micro- and nanoscale spots with discrete elastic moduli from ≈50 to ≈350 MPa. We observed a differential colocalization of FAs to the patterned rigid regions in hMSCs, and that this response was maintained on micrometer and sub-micrometer features, revealing the existence of a sub-micrometer machinery in hMSCs that may be important in the cellular response to local rigidity.

We further assessed the influence of heterogeneous rigidity on differential hMSC function through ingenuity pathway analysis of osteochondral differentiation. Crucially, we noted significant modulation to intracellular signaling processes involved in osteochondral lineage commitment pathways as a function of both spot rigidity and spot size relative to cells cultured under control conditions (unexposed PDMS coupled with chondrogenic or osteogenic growth media). Interestingly, the onset of osteochondral differentiation was induced on heterogeneous rigidity substrates after only 12 h in culture. Elucidating the geometrical and mechanical limits of the cellular mechanoresponse to discrete rigidity will enhance current understanding of in vivo cell behavior in processes such as embryogenesis, healing, and cellular metastasis.[26] In addition, an understanding of the geometrical basis for rigidity sensing will be essential for the design of implants with artificial smart surfaces for optimal cellular interfacial interaction.

PDMS was prepared at a 50:1 ratio of base polymer:accelerating agent and was spin-coated onto standard microscope cover glasses. Samples were cured for 12 h at 70 °C to form optically transparent viscoelastic films, ≈120 nm thick, which were rendered hydrophilic via a 1 min oxygen plasma treatment to facilitate subsequent spin-coating of an electrically conducting layer (AquaSAVE, Mitsubishi Rayon) to suppress charging during e-beam exposure. PDMS substrates were patterned by e-beam exposure using a scanning electron microscope equipped with a Nabity NPGS pattern generator. Patterns were generated on the elastomer surface with e-beam exposure doses ranging from 500 to 3000 μC cm^{-2}, using an accelerating voltage of 30 kV and a beam current of ≈2.5 nA. The absorbed electron energy within the PDMS at the subsurface rigidity gradient is determined by two factors: (i) the incident electron energy (30 keV in this study) and (ii) the scattering of electrons within the elastomer, which depends on the density of the material (schematized in **Figure 1**A). Analysis of Monte Carlo simulations[27] indicated that over 90% of the e-beam energy was absorbed within approximately 3 μm of the PDMS surface (Figure 1B), resulting in a columnar electron scattering profile with a broad spreading base and an energy absorbtion profile that diminished in intensity with increasing depth. Lateral scattering within the top layer was confined to ≈30 nm at 30 keV.

Peak-force microscopy coupled with nanomechanical mapping (PF-QNM) was employed to characterize the change in the elastic properties of the PDMS as a function of e-beam exposure. The PF-QNM experiments were carried out on a Dimension Icon atomic force microscope (AFM) (Bruker-Nano

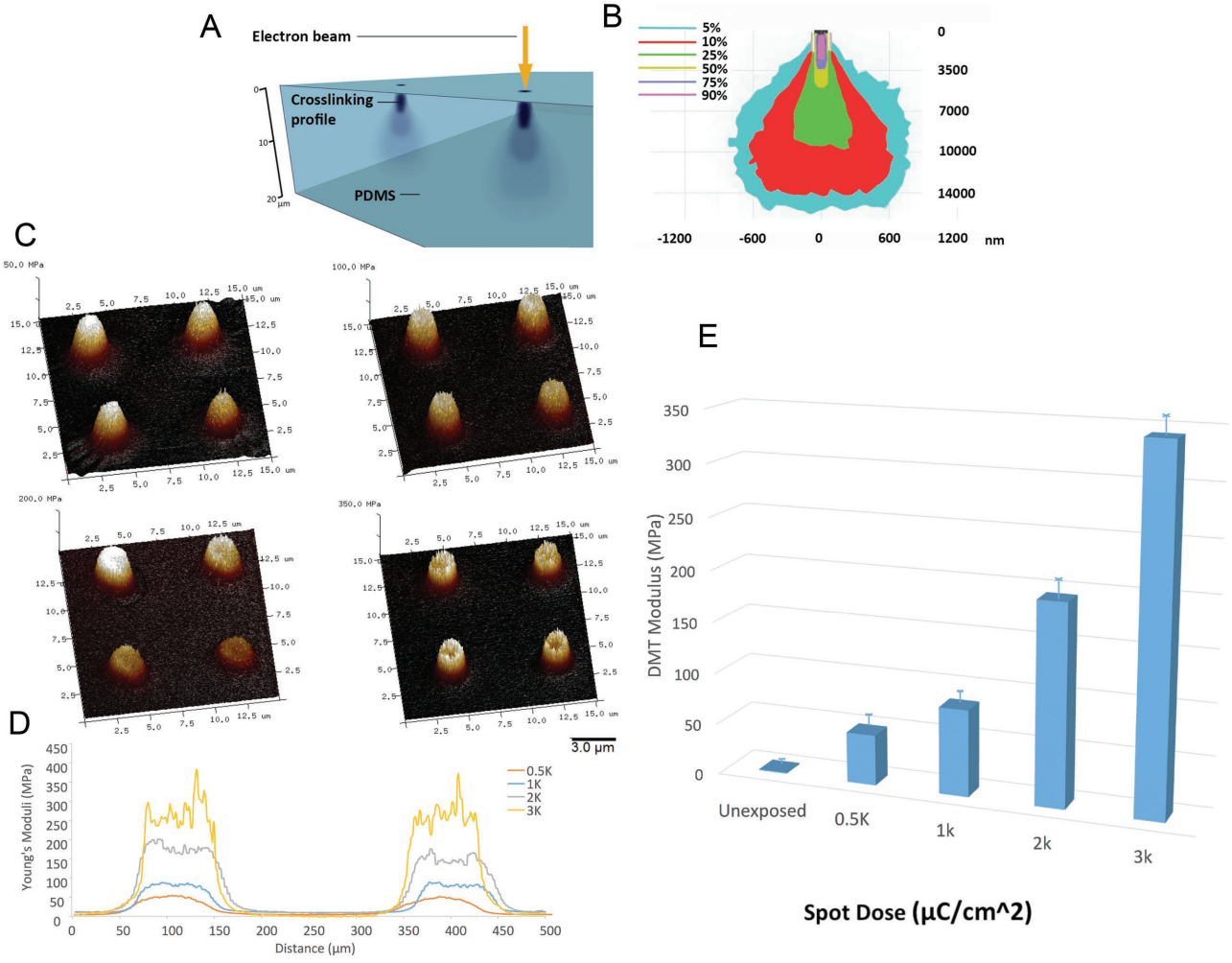

Figure 1. A) Electron-beam interaction with PDMS thin films. A 120 µm layer of PDMS was deposited onto 22 mm square microscopy cover glasses by a spin-coating process. Substrates were treated with an oxygen plasma process and coated with a final polymeric discharge layer (AquaSAVE) prior to e-beam patterning. A focused e-beam was rastered over the substrate surface to create arrays of defined surface features (spots) possessing a subsurface rigidity gradient. B) Monte Carlo simulations identified the electron trajectory and scatter profile in PDMS substrates. C,D) Peak-force quantitative AFM nanomechanical mapping (PF-QNM) of 2 µm diameter spots indicated the e-beam exposure of the PDMS film causes an increase in the elastic modulus of the polymer as a function of e-beam dose. E) The function relating Young's modulus changes to the e-beam exposure dose.

Inc., Santa Barbara, CA) operating in peak-force tapping mode under ambient conditions at a scan rate of 2 Hz and a constant impact force of 5 nN obtained with DNP-10 cantilevers, precisely calibrated through a thermal tune process with resulting spring constants of 0.295 and 0.072 N m^{-1}. Samples with known elastic moduli were used to validate the tip calibration process (low-density polyethylene 10 and 14 MPa and PDMS 1 MPa).[27] The analysis of the Derjaguin–Mueller–Toporov (DMT) modulus was performed via Nanoscope Analysis software.

As mentioned above, the Monte Carlo simulations indicate that most of the electron energy was deposited in the initial ≈3 µm of the PDMS film surface. In PF-QNM, the probe and sample are intermittently brought together to map and distinguish nanomechanical properties of a material - including modulus, adhesion, dissipation, and deformation. As a force curve is recorded for each pixel of the image, the resolution obtained for all the channels was identical to topographical AFM imaging and quantitative data could directly be obtained without postprocessing. The loading force was carefully adjusted so that the tip could effectively indent into the sample and thus give reliable elastic and deformation response and was sufficiently gentle not to wear the tip or damage the sample. The results of the PF-QNM resulting elastic moduli for the electron beam patterned PDMS films are shown in Figure 1C,D. PDMS substrates were exposed to e-beam energies from 500 to 3000 µC cm^{-2} which resulted in a significant increase in the stiffness of the ≈35 kPa unexposed polymer - up to four orders of magnitude (≈350 MPa) with doses of 3000 µC cm^{-2} (Figure 1E).

Concurrent AFM topographical analysis indicated that e-beam exposure of the PDMS surface resulted in the formation of subtle nanometer undulations (Figure S1A,B, Supporting Information), which fell below the limits of cellular topographical sensing.[36] Nevertheless, in order to isolate the possible involvement of the topographical modulation (arising from e-beam-mediated substrate contraction) on cellular function,

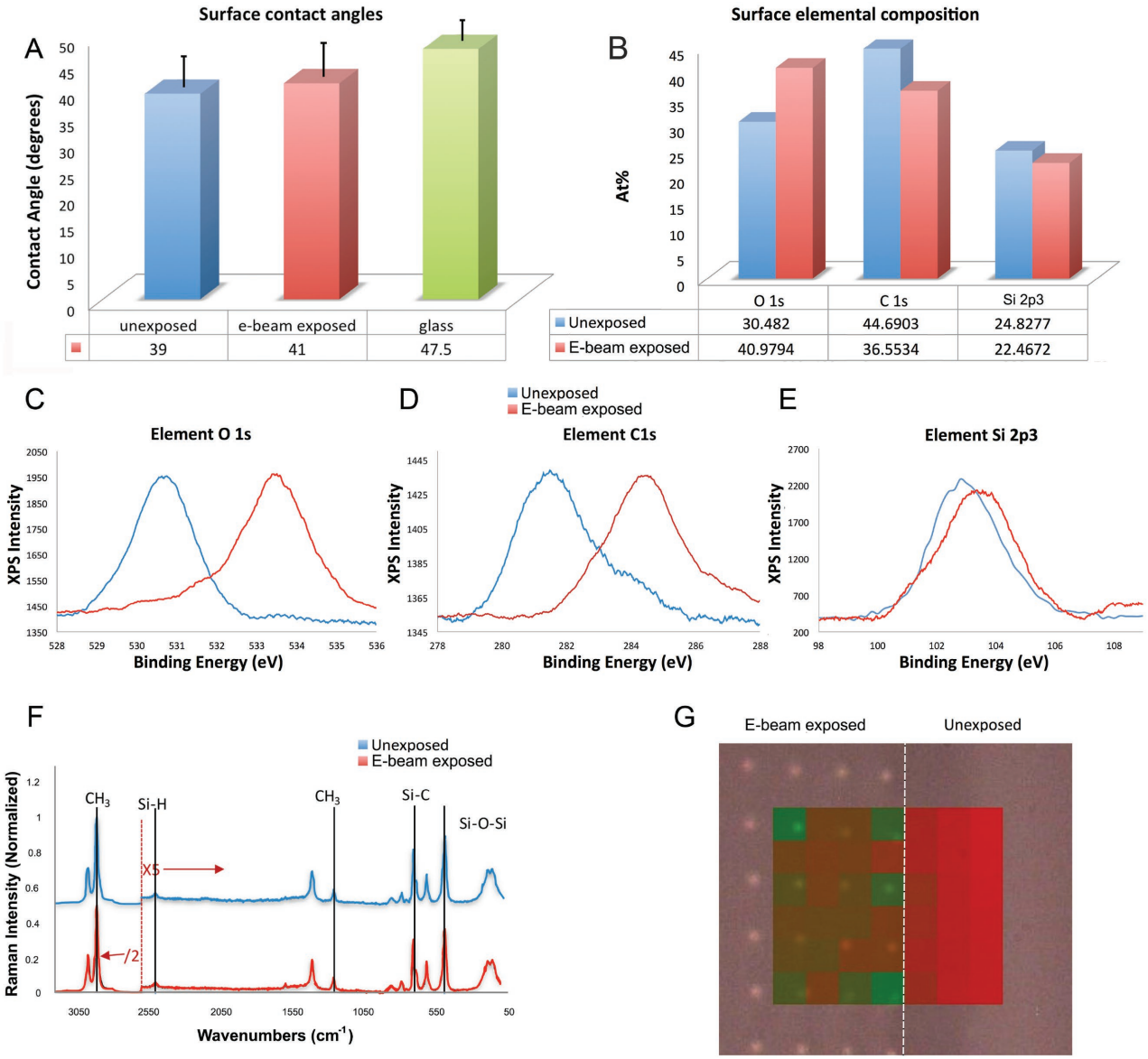

Figure 2. A) Chemical modification of PDMS substrates by focused electron-beam patterning. B) Surface wettability analysis following PDMS treatment with an oxygen plasma. High-resolution X-ray photoelectron spectroscopy of C) O 1s D) C 1s, and E) Si 2p3. F) Raman spectra of e-beam exposed and unexposed PDMS regions. The spectra below 2600 cm^{-1} were enhanced five-fold, while spectra above 2600 cm^{-1} were reduced two-fold, for better visibility of the peaks. G) Component discriminant least squares analysis, using peaks from e-beam exposed (green) and unexposed (red), as the spectra of the components, shows spectral differences on PDMS patterned with 1 µm spots. The figure shows that the peaks that define the control region are also found in the interspot region (red), while the e-beam exposed 1 µm spots are associated with significant peaks (green) that are not present in unexposed regions.

control PDMS substrates were fabricated by imprinting 35 kPa PDMS with a negative PDMS stamp to replicate the topographical undulations formed via e-beam exposure, in a substrate presenting homogeneous rigidity (Figure S1C,D, Supporting Information). Cellular responses to these control substrates as assessed through focal adhesion colocalization to undulations were not observed, indicating that mechanically or topographically induced to these subtle features was not initiated (Figures S2 and 5, Supporting Information).

Samples were cleared of AquaSAVE prior to physicomechanical analysis and the effects of PDMS e-beam irradiation on surface chemistry were assessed prior to in vitro cell experiments to ensure that the modulation of cellular function was exclusively rigidity dependent and not as a result of altered surface hydrophobicity and/or protein adsorption. All analyses were conducted with e-beam exposures of 3000 µC cm^{-2} . The wettability of experimental PDMS substrates was analyzed by contact angle measurements (**Figure 2**A), which confirmed no significant differences between all the experimental materials used in the study. High-resolution XPS of the O 1s, C 1s, and Si 2p3 spectra revealed that e-beam exposure modified the oxygen and carbon composition of the PDMS surface, increasing the

oxygen content from 30.5 to 41% and decreasing the carbon content from 44.7 to 36.5% (Figure 2B). Furthermore, the O 1s values were associated with binding energy peak shifts from 530.75 eV for unexposed PDMS to 533.4 eV following e-beam exposure and the C 1s binding energy shifted from 282.1 for untreated PDMS to 284.85 following e-beam exposure. The Si 2p3 binding energy was also observed to undergo a modest shift from 102.8 to 103.85 eV after e-beam exposure (Figure 2C–E). A full XPS spectrum of exposed and unexposed PDMS is presented in Figure S3A (Supporting Information).

In order to probe the mechanism of e-beam-induced increased rigidity in PDMS, Raman spectroscopy analysis was performed to assess the effects of 3000 μC cm^{-2} dose e-beam exposure on polymer chain cross-linking. PDMS has been well characterized via Raman spectroscopy and characteristic spectral peaks have previously been assigned to specific inter- and intramolecular bonds.[28] Binding energies corresponding to C—Si, C—C, phenyl ring associated sp^2 C, sp^3 C, and adventitious C—O and C=O were observed in both unexposed and exposed surfaces (Figure 2F).

When analyzing subtle differences between spectra, as observed between e-beam exposed and unexposed PDMS samples, multivariate analysis like principal component analysis (PCA) and component discriminant least squares (component DLS) are very useful in identifying differences. Raman mapping of e-beam exposed samples patterned with doses of 3000 μC cm^{-2} to form arrays of 1 μm spots and pristine PDMS samples was carried out using a 3 μm step, with a 534 nm laser. The maps were then post-processed via PCA and DLS analysis to create a ratio of the peak intensities at 490 cm^{-1}/705 cm^{-1} and 2500 cm^{-1}/ 2905 cm^{-1}. Data suggested a 9.4% reduction in the presence of Si—O—Si bonds and a 116% increase in the presence of Si—H bonds on e-beam exposed PDMS. A comparison of the peak intensities at 490 /745 cm^{-1} yielded a similar result to that of the peak intensities fat 490/705 cm^{-1}, indicating a significant increase in chain cross-linking through CH_2—CH_2 linkages or Si—H—Si bridges.[29]

Component DLS analysis using peaks from e-beam exposed (green) and unexposed (red), as the spectra of the components, indicated that the peaks that define the control region were also found in the interspot region (red), while the e-beam exposed spots were associated with significant peaks (green) that were not present in unexposed regions (Figure 2G). Following e-beam exposure with doses of 3000 μC cm^{-2} significant changes were observed in the intensities of Si—O—Si stretches at 490 cm^{-1}, Si—C stretches at 705 cm^{-1}, Si—H stretch at 2500 cm^{-1}, —CH_2—CH_2— bending at 745 cm^{-1}, CH_3 bending at 858 cm^{-1}, and CH stretching at 2905 cm^{-1}. A full assignment of peaks and the spectra can be found in Figure S3B (Supporting Information).

To assess protein adsorption to heterogeneously patterned rigidities, ≈35 kPa PDMS substrates were patterned with an array of 2 μm spots possessing an elastic modulus of ≈350 MPa (formed with an e-beam dose of 3000 μC cm^{-2}). The protein adsorption distribution was determined from the fluorescence intensity profile of labeled fibronectin versus the bright-field differential interference contrast (DIC) intensity of the e-beam exposed materials and was analyzed with ImageJ. The bright-field DIC intensity increased sharply at the irradiated regions, demonstrating that e-beam-exposed PDMS causes minimal lateral scattering during irradiation and indicating the presence of diffractive modification, consistent with intense cross-linking of the elastomer, as discussed above. On the other hand, the fluorescence intensity profile was unchanged at the sites of e-beam exposure, indicating a uniform distribution of protein adsorption on the patterned substrates (**Figure 3**C). We note that the surfaces were not subjected to a protein adsorption process prior to cell seeding.

To study the cellular response to heterogeneously patterned rigidities, PDMS substrates were patterned with an array of spots with diameters ranging from 100 to 2000 nm and with elastic moduli ranging from ≈50 kPa (control) to ≈350 MPa (e-beam dose of 3000 μC cm^{-2}). The interspot distance was modulated proportionally with spot diameter (edge–edge spacing was maintained at 3ϕ) in order to ensure that the cells were exposed to a constant rigid/soft ratio. Substrates were sterilized in 70% ethanol and washed in phosphate-buffered saline (PBS) solution before seeding of hMSCs derived from human bone marrow aspirates. Cells were cultured on experimental and control substrates for 12 h before fixing and preparing for immunocytochemistry. Cells were immunostained for the FA protein paxillin and for filamentous actin (rhodamine-conjugated phalloidin) and analysis of FA colocalization on the electron-beam patterned samples was performed with ImageJ (Figure S4, Supporting Information).

Analysis of FA formation on exposed spot regions showed that FA colocalized to the e-beam exposed spots, and the degree of colocalization increased with applied electron beam dose (Figure 3A–C). On substrates patterned with ≈350 MPa spots measuring 2 μm in diameter, MSCs formed punctate FAs that colocalized significantly with the underlying exposed region. This effect was observed to diminish with decreasing spot rigidity (Figure 3A–C). On less stiff spots, elongated FAs were observed to initiate at the irradiated regions yet extended onto the "soft" 35 kPa unexposed interspot regions, and colocalization was eliminated with decreasing spot rigidity (Figure S2, Supporting Information). FA colocalization to spots of increased rigidity was also coupled with an increase in the fluorescence signal intensity of paxillin staining (Figure S5A, Supporting Information). Varying the spot rigidity was not observed to significantly modulate cellular spreading however (Figure 3D), yet spots with elastic moduli greater than 100 MPa induced significant reductions in the mean cellular total FA area (Figure 3E). For statistical significance of focal adhesion colocalization as a function of spot elastic modulus see Table S1 (Supporting Information).

Additional analysis of FA colocalization to rigid spots revealed that punctate FA colocalization was dependent on spot size. On the ≈350 MPa spots, reducing the exposed spot diameter from 2 μm to 100 nm significantly decreased FA colocalization (**Figure 4**A–C). By decreasing the spot diameter and interspot spacing, colocalized, punctate FAs became less frequent (Figure S6, Supporting Information); rather, FAs were observed to bridge between multiple spots indicating FA sensing machinery can initiate discrete protein reinforcement along the FA plaque. This was also observed as an increase in the fluorescence signal intensity of paxillin staining on spots of increased diameter (Figure S5B, Supporting Information).

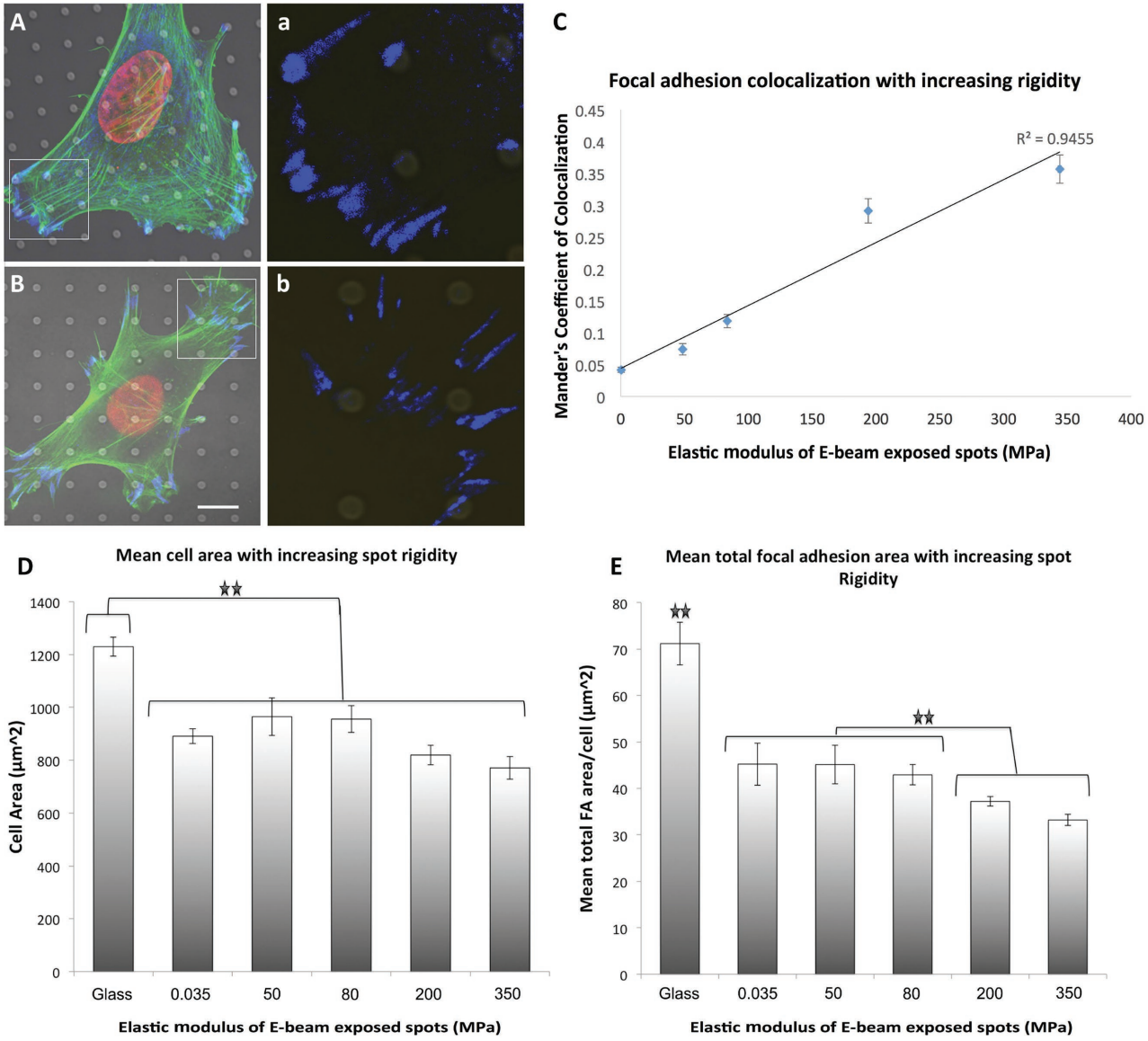

Figure 3. hMSC focal adhesion formation on 2 µm spots of varying rigidity. A) Electron-beam spots of ≈350 MPa induced differential focal adhesion colocalization in hMSCs. B) This effect was lost on ≈50 MPa spots. High-magnification inset of paxillin staining within the boarded area indicated in (a) and (b). C) e-beam exposure induced a linear increase in focal adhesion colocalization to spots of altered rigidity. D) Cellular spreading was not affected in MSCs cultured on 2 µm diameter spots of modulated rigidity. E) Significant changes in mean FA area were induced by increasing the elastic modulus of 2 µm diameter spots. For statistical analysis of significance, see Tables S1 and S2 (Supporting Information). Results are SEM, green = actin, blue = paxillin, red = nucleus, bar = 10 µm.

Again, varying the spot diameter was observed to significantly modulate total FA area, yet not cellular spreading. However, varying the spot size was observed to affect cellular motility (Movies M1–M3, Supporting Information). Specifically, cell velocity and mean migration distance were significantly reduced on substrates patterned with dots >500 nm in diameter (Figure S6, Supporting Information). For a statistical significance of focal adhesion colocalization as a function of spot diameter, see Table S2 (Supporting Information).

The effects of heterogeneous rigidity as a function of both spot rigidity and diameter on differential hMSC function were investigated, with a focus on the regulation of early signalling events in chondrogenesis and osteogenesis. Cells were seeded onto experimental substrates for 12 h preceding RNA isolation. To perform high-throughput quantitative genomic analysis on 1 mm^2 electron-beam patterned samples, real-time quantitative polymer chain rection (qPCR) analysis was conducted using Fluidigm integrated microfluidic circuit analysis, capable of performing 9216 simultaneous qPCR experiments with nanoliter quantities. Fold changes were expressed relative to cells cultured either in chondrogenic or osteogenic media on unexposed PDMS substrates. Ingenuity pathway analysis (IPA) identified 78 genes, which underwent statistically significant modulation in response to the heterogeneous rigidity patterns.

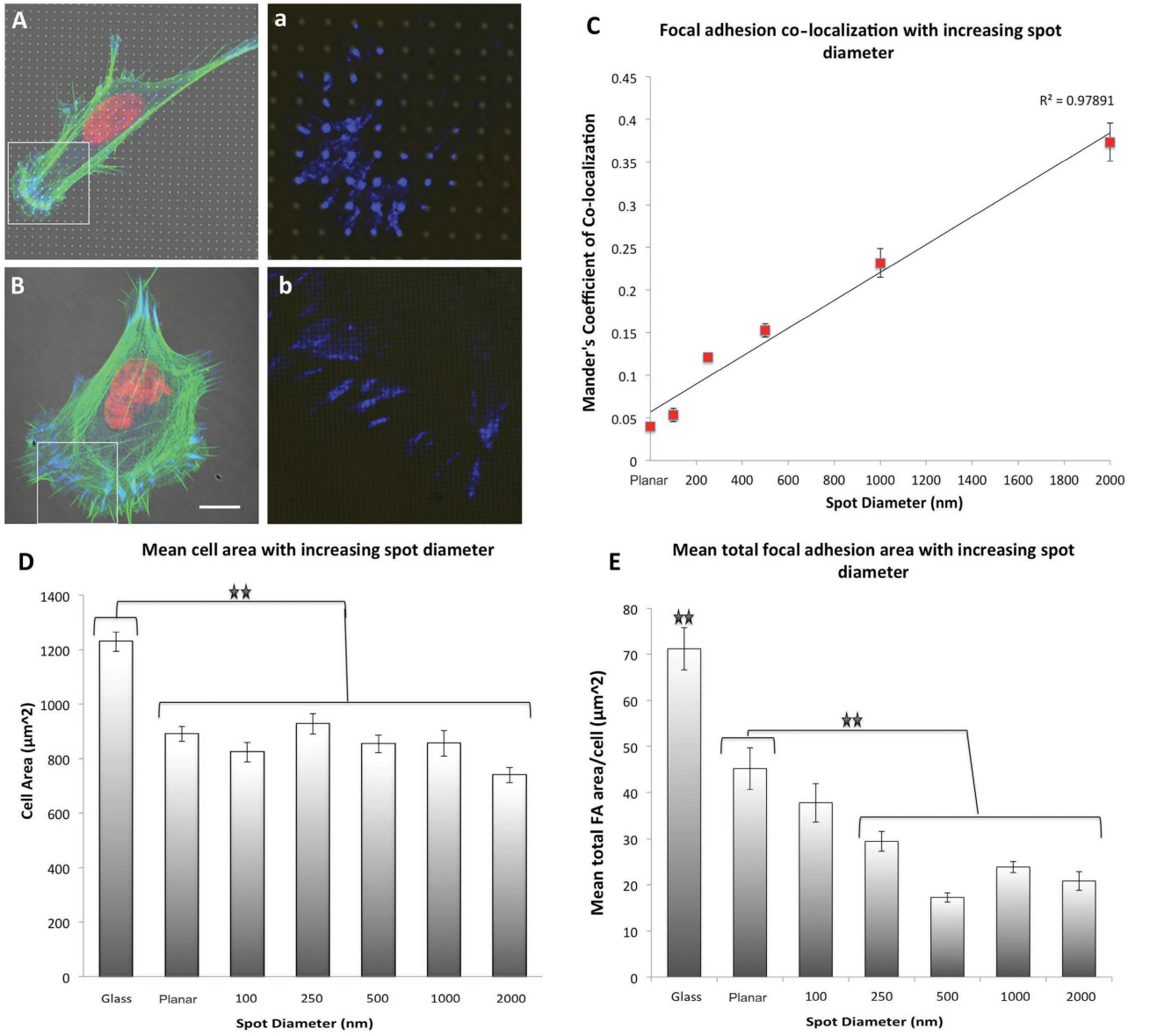

Figure 4. hMSC focal adhesion formation on ≈350 MPa spots of varying diameter. A) 1 µm spots of ≈350 MPa (formed with doses of 3000 µC cm^{-2}) induced differential focal adhesion colocalization in hMSCs as a function of spot diameter. B) This effect was lost on 100 nm spots, high-magnification inset of paxillin staining within the boarded area indicated in (a) and (b). C) Mander's coefficient of colocalization indicated a linear increase in FA colocalization to the e-beam exposed regions with increasing spot diameter, up to a miximum at 2 µm. D) Cellular spreading was not significantly different in MSCs cultured on spots of modulated rigidity as a function of spot diameter relative to unexposed PDMS, yet significant reductions in cell spreading were noted relative to hMSCs cultured on glass control substrates. E) Significant reductions in mean FA area were also induced by reducing the spot diameter. For statistical analysis of significance, see Table S2 and S3 (Supporting Information). Results are SEM, green = actin, blue = paxillin, red = nucleus, bar = 10 µm.

These genes were attributed to specific signalling pathways which were assigned an activation *z*-score to infer signaling pathway activation (**Figures 5** and **6**). Analysis of FA-associated signaling pathways in hMSCs cultured on 2 µm diameter spots of increasing rigidity revealed that FA formation was deactivated on unexposed substrates and substrates possessing ≈350 MPa spots. FA deactivation was predominantly due to deactivation of vinculin signalling relative to hMSCs cultured under control chondrogenic and osteogenic conditions (Figures S7 and S8, Supporting Information).

Functional pathway analysis of hMSCs cultured on 2 µm diameter spots of increasing rigidity indicated rigidity-dependent activation of signaling pathways involved in cell survival, angiogenesis, differentiation of chondrocytes, and the development of cartilage tissue relative to cells cultured on unexposed substrates in the presence of chondrogenic induction media. Conversely, significant deactivations of pathways attributed to cellular apoptosis and cell mineralization were observed. Interestingly, deactivation of signaling pathways involved in cell survival, cell proliferation, and angiogenesis

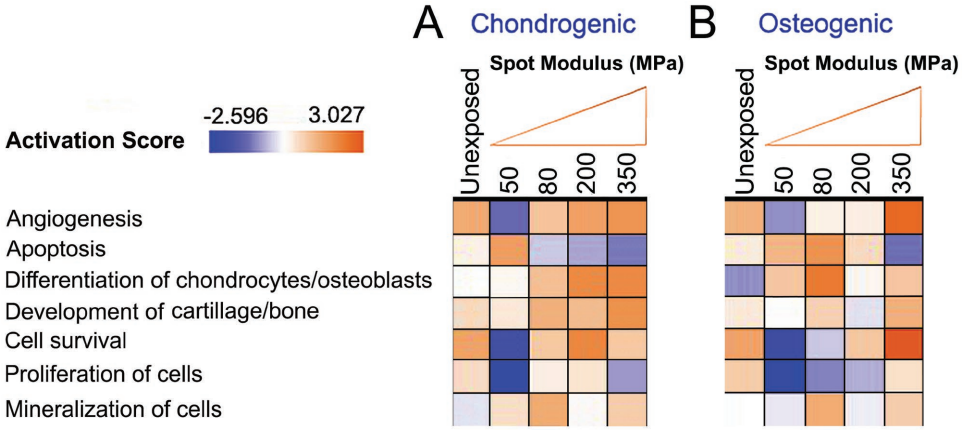

Figure 5. Functional analysis of hMSCs cultured on PDMS substrates patterned with 2 µm spots of increasing rigidity for 12 h. Functional pathway analysis of hMSCs cultured on 35 kPa PDMS substrates e-beam patterned with 2 µm spot revealed significant activation of signaling pathways as a function of spot rigidity relative to cells cultured on unexposed homogenous rigidity substrates in A) chondrogenic and B) osteogenic media. Red indicates an increase in pathway activation and blue indicates a decrease in pathway activation relative to controls as shown in the activation score bar. Statistical significance of pathway modulation was calculated via a right-tailed Fisher's exact test.

was noted predominantly in hMSCs cultured on 2 µm diameter spots possessing an elastic modulus of ≈50 MPa (500 C cm^{-2} exposure dose) (Figure 5A). Similar changes were noted in MSC populations relative to cells cultured on unexposed substrates in the presence of osteogenic induction media (Figure 5B). Pathways associated with chondrocyte and osteoblast development appeared to be rigidity sensitive, and a linear increase in the prediction of chondrocyte differentiation was observed as a function of spot dose associated with upregulation of cartilage development genes, BMP2, BMP4, RUNX2, SOX9, and BMPR2 (Figure S9, Supporting Information). A nonlinear response was observed in the prediction of osteogenesis however with significant increases occurring with cells culture on ≈80 MPa spots, Here, upregulation of osteocyte development genes BMP2, RUNX2, coupled with downregulation in HIFA, SMURF1, and TWIST1 was noted (Figure S10, Supporting Information) (fold-change values; Table S3, Supporting Information).

As the observed influence of heterogeneous rigidity on FA colocalization was lost with spot sizes <500 nm, modulations to differential cell function as a function of spot diameter were investigated with spot diameters ranging from 500 nm to 2 µm. Analysis of FA-associated signaling pathways in hMSCs cultured on ≈350 MPa spots revealed that FA signaling pathways were deactivated on unexposed substrates and substrates possessing all investigated spot diameters. FA deactivation was predominantly due to downregulations in the expression of vinculin, paxillin, SRC, and integrin 1 relative to control chondrogenic and osteogenic conditions (Figures S11 and S12, Supporting Information).

PDMS substrates patterned with ≈350 MPa spots with a diameter <2 µm demonstrated significant deactivation of

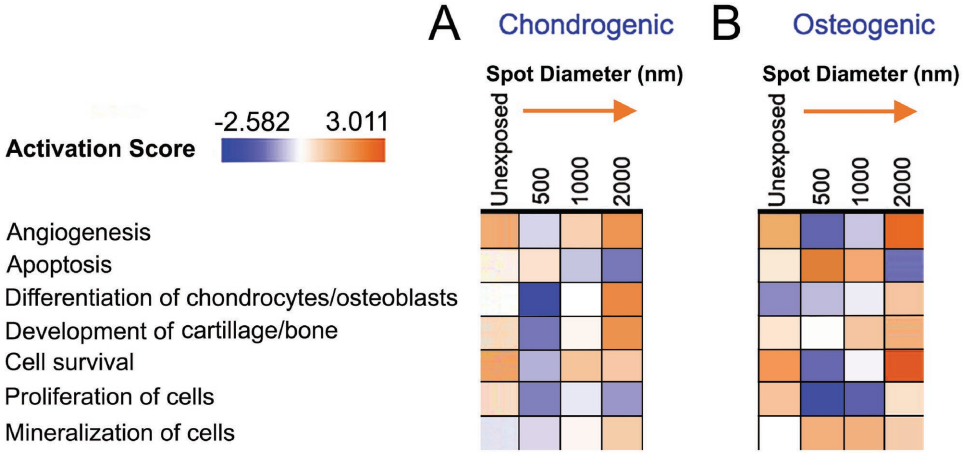

Figure 6. Functional analysis of hMSCs cultured on PDMS substrates patterned with ≈350 MPa spots of increasing spot diameter for 12 h. Functional pathway analysis of hMSCs cultured on e-beam patterned spots with diameters ranging from 500 to 2000 nm revealed significant activation of signaling pathways as a function of spot size relative to cells cultured on control homogeneous rigidity substrates in A) chondrogenic and B) osteogenic media. Red indicates an increase in pathway activation and blue indicates a decrease in pathway activation relative to controls as shown in the activation score bar. Statistical significance of pathway modulation was calculated via a right-tailed Fisher's exact test.

pathways associated with differential cell function. Relative to hMSCs cultured in the presence of chondrogenic induction media, cells cultured on 2 μm diameter spots demonstrated enhanced angiogenic signaling, enhanced chondrocytic differentiation, enhanced cartilage development, and enhanced cell survival. These effects were also noted in cells cultured in 1 μm spots, yet to a lesser degree, however these pathways were significantly deactivated in hMSCs cultured on 500 nm diameter spots (Figure 6A). Similarly, relative to hMSCs cultured in the presence of osteogenic induction media, cells cultured on 2 μm diameter spots demonstrate enhanced angiogenic signaling, enhanced osteospecific differentiation, enhanced bone development, and enhanced cell survival (Figure 6B). Pathways associated with chondrocyte and osteoblast development also appeared to be sensitive, to the spot diameter and a linear increase in the prediction of chondrocyte differentiation was observed as a function of spot size associated with upregulations of cartilage development genes, BMP2, BMP4, RUNX2, SOX9, and BMPR2 (Figure S13, Supporting Information). A nonlinear response was observed in the prediction of osteogenesis however with significant increases in the prediction of osteogenesis noted only with spot sizes of 2000 nm, Here, upregulation of osteocyte development genes BMP4, BMP2, RUNX2, ACVR2B, NOTCH1, SMURF1, and JAG1 was noted (Figure S14, Supporting Information) (fold-change values; Table S4, Supporting Information).

Here, we describe a direct-write e-beam process to induce localized cross-linking of thin-film PDMS substrates and employ this technique to explore the effects of micrometer to nanoscale heterogeneous surface rigidity on differential hMSC function. A similar increase in PDMS cross-linking, accompanied by increased rigidity, as a result of exposure to a Ga^+ ion beam, was recently reported by Liu and Fu.[30] Ion beams are typically used to modify the structure of materials (i.e., by sputtering or by ion implantation), and in that work, the resultant changes to the PDMS mechanical properties could be attributed to both modification of the PDMS polymer structure as well as the incorporation of Ga into the polymer. Similarly, a previous study by Bowen et al. explored the effect of e-beam exposure on the mechanical properties of uncrosslinked PDMS with an aim to validating PDMS as a potential e-beam resist.[31] Interestingly, this study reported very similar mechanical responses of the prepolymer to e-beam exposure to those reported herein. Conversely, direct-write focused e-beam patterning, which has not previously been explored to produce geometrical patterns of increased rigidity on viscoelastic PDMS substrates was employed in this study. Significant increases to the elastomer modulus was observed to scale with increased e-beam dose, effectively increasing the materials' elastic modulus by four orders of magnitude, from ≈35 kPa to ≈350 MPa.

The analysis of e-beam-induced modulation of elasticity was accomplished via peak-force quantitative AFM, enabling mapping of the substrate mechanical properties with nanoscale resolution. Direct-write e-beam patterning to control the size and geometric arrangement of the spots facilitated the engineering of substrata with defined distributions of heterogeneously increased rigidity with dimensions ranging from the micrometer to the nanoscale. Although spot features were explored in this study, ongoing studies are investigating the effects of anisotropic rigidity features on cell function (Figure S15, Supporting Information) and it is important to indicate the versatility of e-beam patterning in generating complex and arbitrary feature shapes,[32] in conformations ranging from ordered to random.[33]

In contrast to the observations of Russell et al.,[25] it was noted in this study that the PDMS chemistry was affected by focused e-beam exposure; in particular, the measured surface carbon content was reduced and the creation of SiO_2 was confirmed by a shift in the peak positions of the SI 2p and the O 1s binding energy signals (Figure 2F). This was also reported in a previous study by Schnyder et al. which described a very similar reduction in carbon and increase in oxygen composition in PDMS following exposure to UV light.[34] Subsequent degradation of the polymer was confirmed through X-ray photoelectron spectroscopy (XPS), and corresponding binding energy shifts reached values corresponding to SiO_2. The C 1s binding energy for untreated PDMS of 282.1 shifted to 284.85 following e-beam exposure and the Si 2p binding energy from 102.8 to 103.85 eV after e-beam exposure. This peak position corresponds exactly with literature values of 102.1–103.4 following UV exposure. With respect to O 1s values the corresponding peak shifts from 530.75 eV for unexposed PDMS to 533.4 eV following e-beam exposure again were identical to previously reported studies with UV exposure of PDMS.

We hypothesized that the observed increase in PDMS rigidity as a function of e-beam exposure dose was due to a dose-dependent increase in PDMS chain cross-linking. Indeed, Raman spectroscopy suggested a 9.4% reduction in the presence of Si—O—Si bonds and a 116% increase in the presence of Si—H bonds on e-beam-exposed PDMS indicating a significant increase in chain cross-linking through CH_2—CH_2 linkages or Si—H—Si bridges.[29] Critically, we did not observe differential fibronectin adsorption on heterogeneous rigidity substrates a finding also verified in a similar study employing photo-crosslinking of microdomains in a hydrogel system to create heterogeneous rigidity substrata.[35] This is important as it indicates that the observed FA colocalization effects could not be attributed to differences in protein adsorption between the exposed and unexposed regions which has been shown previously to modulate the reinforcement of FAs,[36] the dynamic turnover of FA associated proteins,[37] and integrin-mediated signaling activity.[38]

Focal adhesions play dual physiological functions—as physical structures that direct and regulate tissue and organ morphogenesis through mechanical cellular coupling to the ECM, and as bidirectional mechanosensors that modulate intracellular signaling events. The mechanisms of adhesion-mediated sensing of the physical properties of the ECM are yet to be resolved, however cells are exquisitely sensitive to the physical state of the local environment and studies with bulk systems of rigidity have shown that cells respond dynamically to rigidity gradients, and migrate from regions of lower to higher rigidity, in a process termed durotaxis.[18,39]

Major differences in intracellular tension, FA reinforcement and density are reported in cells cultured on surfaces with bulk rigidity values in the sub-kPa to kPa range, relative to cells cultured on surfaces with bulk rigidity in the kPa to MPa range.[5,40] However, conflicting hypotheses exist on the

mechanisms of bulk-rigidity-mediated changes to FA reinforcement and subsequent cell function. It is known that FA reinforcement and induction of actin organization require certain threshold densities of adhesion ligands,[41,42] however the existence of a minimum length scale at which cells can sense rigidity has not yet been established. Our results demonstrate clearly that the formation of FAs in hMSCs cultured on substrates with heterogeneous rigidity is dependent both on feature stiffness and size. The formation of discrete punctate FAs coupled with an increase in paxillin recruitment on spots 1 μm in diameter indicate that this length scale lies between 500 nm and 1 μm. Critically, paxillin recruitment to FAs and subsequent phosphorylation has been identified as essential for high FA traction over a broad range of ECM rigidity.[43]

In agreement with a recent study by Monge et al., it was observed that on spots posessing a rigidity <350 MPa, FAs did not extend from the spot center, but rather initiated at the spot boundary.[35] It was also observed that on spots ≤1 μm in diameter, FAs had a tendency to extend paxillin domains, and single FAs were associated with multiple rigid spots. This behavior is similar to that observed by Arnold et al. with cells plated on adhesive patches of RGD peptide.[44] That study concluded that adhesive areas of 1 μm^2 could support the formation of sufficiently mature FAs to withstand the applied load per patch necessary for cell spreading. In contrast, cells were observed to couple to adjacent paxillin domains through a single actin bundle if adhesive patches were ≤500 nm, in order to mechanically stabilize adhesion and facilitate cell spreading.[44] Our results suggest that rigidity-mediated adhesion is regulated by the same machinery that governs FA assembly and reinforcement and that this machinery is capable of recognizing localized discrepancies in matrix rigidity.

The minimum scale for FA initiation and early integrin clustering events in response to discrete rigidity structures is unknown. A recent study by Yang et al. explored the influence of heterogeneous rigidity on hMSC adhesion through a photoreactive hydrogel system employing copolymerizing PEG monoacrylate (PEGA) with a photodegradable PEG diacrylate (PEGdiPDA). Using photolithographic masks, cell culture substrates were synthesized through a UV photodegradation process at 365 nm to yield hydrogels possessing discrete regions of reduced rigidity, from 9.6 to 2.3 kPa. Owing to the resolution limits of photolithography the smallest future size obtainable with this approach was limited to 2 μm^2. Interestingly, it was also noted in this study that paxillin intensity was increased in FAs formed on regions of increased rigidity.[45] Further studies employing stiff islands of ≈36 μm^2 concluded that although the islands were too large to address the minimal adhesion area required to trigger FA formation, as long as adhesion sites are well-anchored to resist traction forces, the area of adhesion is limited only by the minimal area required to support focal complex initiation.[46] Recently, Meacci et al. reported that it is the local FA contraction mechanics mediated by myosin II and α-actinin, and not intracellular tension that plays the central role in FA reinforcement in response to local rigidity sensing.[47] We suggest that this localized contractile unit is a prime candidate for this role and our results set the size scale for this unit.

Direct mechanical cues have been shown to play a significant role in regulating osteochondral differentiation[48] and it was interesting to note that substrates possessing heterogeneous rigidity with spot rigidities >50 MPa were able to increase focal adhesion colocalization and initiate the activation of differential functional pathways in hMSCs followed only 12 h of culture relative to cells cultured in osteospecific or chondrospecific induction media. In this study IPA pathway analysis revealed several functional pathways linked to osteochondral growth and differentiation induced by upregulation of BMP-2/-4, Rac1, RhoA, and ROCKII which influence RUNX2 and SOX9 expression.[49] Critically, the activation of pathways associated with osteochondral differentiation were noted predominantly on 2 μm spots posessing a modulus of ≈350 MPa, and this effect was eliminated on substrate with spots diameters <500 nm, which can be argued effectively presented a bulk, homogenous rigidity of ≈350 MPa.

Tissues do not represent bulk rigidity systems, but rather are composed of heterogeneous distributions of particles, and fibers of varying rigidity. We have developed a new type of biomimetic surface comprising regions of heterogeneous rigidity at the micro- and nanoscale by writing on PDMS films with an electron beam. Peak-force quantitative AFM nanomechanical mapping of these surfaces revealed a substantial increase in the Young's modulus of the elastomer as a function of the e-beam exposure. By monitoring cellular response to these surfaces, we have demonstrated in a planar system that the apperatus of cellular rigidity sensing can respond to discrete sub-micrometer discrepancies in the matrix rigidity, and that FAs demonstrate intrinsic "local" reinforcement in response to rigid features measuring ≳500 nm in diameter. At ≲500 nm, the ability to sense the rigid features is completely lost. This contrasts with cellular response to other physical cues, such as topography[12,38] and geometry,[42,44] where cells respond to features well into the nanoscale. Different cell types respond differently to rigidity however and may have different spatial and rigidity requirements to elicit differential responses.

The versatility of the patterning system presented here can be applied to a broad range of cellular systems in order to elucidate the specific requirements for each, and in engineering next-generation biomaterial interfaces to control cell function and i.e. maintain cell stemness. Understanding these responses can be used to inform the design of new types of tissue scaffolds and may have implications in the treatment of cancer and other diseases.

Experimental Section

Substrate Fabrication: Microscope cover glasses (Corning, NJ) (22 mm^2 No. 0) were cleaned for 12 h in a 1% v/v solution of the detergent MICRO-90 (International Products, NJ), rinsed in reverse osmosis water (ROH_2O) and blown-dry in a stream of filtered nitrogen. Sylgard 184 PDMS (Dow Corning, MI) was mixed with the supplied accelerating agent at a ratio of 50:1 for 5 min and degassed under vacuum for 10 min at 5 Torr. PDMS (0.5 mL) was applied to the microscope cover glasses and spin-coated for 45 s at 1000 rpm and an acceleration of 400 rpm s^{-1} to form a uniform film. PDMS-coated cover glasses were cured for 17 h at 70 °C before further processing. Substrates were subjected to an oxygen plasma in a tabletop Harrick PDC32G plasma cleaner for 10 s at a RF power of 18 W to induce surface hydrophilicity. Samples were next coated with a conductive discharge layer to facilitate e-beam exposure. A 5 nm thick discharge layer was applied to the substrates by spin-coating

100 µL of AquaSAVE (Rayon, Mitsubishi) for 45 s at 4000 rpm and an acceleration of 400 rpm^2. Samples were stored at RT until e-beam exposure.

Direct-Write Electron-Beam Patterning: The PDMS substrates were patterned by e-beam exposure using a scanning electron microscope (FEI XL 30 Sirion) equipped with a Nabity NPGS pattern generator. A 1 mm^2 area consisting of an arrays of spots with diameters ranging from 100 nm to 2 µm were written onto the substrate surface at doses from 500 to 3000 µC cm^{-2}, an accelerating voltage of 30 kV and a beam current of ≈2.5 nA. Substrates were cleared of AquaSAVE in deionized water for 3 × 5 min and allowed to air dry for 30 min.

Topographical control substrates were fabricated by casting PDMS onto directly e-beam written samples to create negative template. Briefly, e-beam written samples were prepared with doses of 3000 µC cm^{-2} and the patterned area isolated with a glass cloning-ring. PDMS with a base:accelerator ratio of 5:1 was introduced into the cloning ring and allowed to cure overnight at RT. The inverse cloning-ring/PDMS shim was subsequently removed at −80 °C from the direct e-beam written pattern and used for the casting of topographical replicas. Topographical PDMS substrates prepared as above were cast onto the PDMS template overnight to yield topographically modified, yet mechanically homogeneous PDMS substrates.

Surface Characterization: Monte Carlo simulations of electron trajectory in PDMS were conducted with Casino software.[50] Surface physical modification was characterized by nanoindentation, optical profilometry, and scanning electron microscopy measurements. Chemical modification was analyzed by water contact angle, angle, XPS, and confocal laser scanning microscopy measurements. Planar control materials were also subjected to a plasma treatment as described above.

Quantitative AFM Nanomechanical Mapping: The PF-QNM experiments were carried out on a Dimension Icon AFM (Bruker-Nano Inc., Santa Barbara, CA) operating in peak-force tapping mode under ambient conditions at a scan rate of 2 Hz and a constant impact force of 5 nN with DNP-10 cantilevers, precisely calibrated through a thermal tune process with resulting spring constants of 0.295 and 0.072 N m.$^{-1}$ Samples with known elastic moduli were used to validate the tip calibration process (low-density polyethylene 10 and 14 MPa and PDMS 1 MPa).[27] The analysis of the DMT modulus was performed via Nanoscope Analysis software.

Raman Microscopy: Chemical characterization of the substrates was carried out using a Renishaw inVia Raman microscope. Spectra of the control and e-beam exposed regions were collected using a 534 nm laser (5% laser power, 10 s exposure time, 1 acquisition, 50× objective) with a high confocality pinhole to reduce the spot size to under a micrometer, so as to collect data from individual spots and prevent interference patterns. Spectra in the range of 50–3200 cm^{-1} were obtained using extended grating, or in static mode, centering the grating at 950 and 2500 cm^{-1} . Raman maps of the samples were obtained by scanning a region with a 3 µm step. The measurements were made under focused tracking to obtain optomised Raman scattering. Component DLS analysis and PCA of the maps obtained were carried out to differentiate between Raman spectra.

Contact Angle Measurements: Surface wettability analysis was carried out at room temperature using 8 µL water droplets with a model 100_00 contact angle goniometer (Rame-Hart, Inc.). Values were averages measurements obtained from more than three different samples and more than three different locations on each sample.

X-Ray Photoelectron Spectroscopy: XPS spectra were recorded with PHI 5500 model spectrometer equipped with an Al K monochromator X-ray source run at 15 kV and 23.3 mA, a hemispherical electron energy analyzer and a multichannel detector. The test chamber pressure was maintained below 2 × 10^{-9} Torr during the spectrum acquisition. Low-energy electron flood gun was used to neutralize possible surface charging. The XPS BE was internally referenced to aliphatic main C 1s peak (BE = 284.6 eV). Survey spectrum was acquired at an analyzer pass energy of 93.9 eV and BE resolution of 0.8 eV, while the high-resolution spectrum was acquired with a pass energy of 23.5 eV and BE resolution 0.05 eV. Angle-dependent XPS was performed by rotating the sample holder to the desired take-off angle (the angle between the surface normal and the detector) through a motor. Spectrum was fitted by a Gaussian–Lorentz (BE) was internally referenced to aliphatic main C 1s peak function after subtracting a striped background using the PHI data processing software package under the constraint of setting reasonable BE shift and characteristic full width at high maximum (FWHM) range. Atomic concentration was calculated by normalization of the peak area to the elemental sensitivity factor data provided by PHI database.

Protein Adsorption Assay: Surface adsorption of fibronectin was analyzed by fluorescence microscopy. Human fibronectin (Sigma Aldrich) was conjugated directly to Alexa Fluor 488 (Invitrogen) by protein dialysis according to manufacturer instructions (Thermo Scientific). Exposed substrates were prepared as above and immersed in PBS containing 0.5 µg mL^{-1} fluorescent fibronectin. Samples were coated for 18 h before being washed in PBS (3 × 5 min) and mounted for microscopy.

Cell Culture: Substrates were sterilized by successive rinsing in 70% ethanol (3 × 5 s) followed by PBS (3 × 5 s). hMSCs derived from human bone marrow aspirates were isolated using a protocol previously described.[51] hMSCs were cultured in complete medium (MEM alpha, GlutaMAX supplemented with 10% fetal bovine serum and 1% penicillin/streptomycin) and maintained at 37 °C in a humidified atmosphere containing 5% CO_2. Cells were expanded to passage 2 following one week of culture and subsequently trypsinized in TrypLE Express dissociation medium (Invitrogen) and seeded onto untreated experimental and planar control tissue culture plates at a density of 1 × 10^4 cells per sample in 1 mL of complete medium. Cells were maintained at 37 °C with a 5% CO_2 atmosphere in Dulbecco's modified Eagle's medium (Gibco) supplemented with 10% fetal bovine serum (Gibco), 1% L-glutamine, and 100 IU mg^{-1} penicillin/streptomycin (Invitrogen). To induce chondrogenesis, cells were subjected to chondrogenic induction media (Lonza, Switzerland) containing dexamethasone, ascorbate, ITS+supplement, GA-1000, sodium pyruvate, proline, and L-glutamine, supplemented with 10 ng mL^{-1} TGF-β3 (Lonza). For osteogenic induction, cells were cultured in osteogenic basal media supplemented with L-glutamine, ascorbate, dexamethasone, penicillin/streptomycin, MCGS, and β-glycerophosphate (Lonza, Switzerland).

Fluorescent Labeling: Following 12 h of culture on experimental and control substrates, hMSCs cultures were fixed in 4% paraformaldehyde in PBS, with 1% sucrose at 37 °C for 5 min. Once fixed, the samples were washed with PBS. Samples were permeabilized with buffered 0.5% Triton X-100 (10.3 g sucrose, 0.292 g NaCl, 0.06 g $MgCl_2$, 0.476 g [4-(2-hydroxyethyl)-1-piperazineethanesulfonic acid] (HEPES), 0.5 mL Triton X-100, in 100 mL water, pH 7.2) at 4 °C for 5 min. Nonspecific binding sites were blocked with 1% bovine serum albumin (BSA) in PBS at 37 °C for 15 min and subsequently incubated for 2 h with anti-paxillin monoclonal anti-human IgG raised in mouse (1:200, B.D Biosciences, Sparks, MD). Nonspecific charges (e.g., remaining aldehyde) were neutralized with 0.5% Tween 20/PBS (5 min × 3) to minimize background labeling. A secondary, fluorescein isothiocyanate-conjugated antibody was added, in 1% BSA/PBS (1:50, Vector Laboratories, Burlingame, CA) at 4 °C for 1 h and simultaneously, rhodamine-conjugated phalloidin was added for the duration of this incubation (1:50, Molecular Probes, OR). Substrates were given a final wash in PBS (5 min × 3). Samples were mounted in Vectorshield mounting medium for fluorescence (Vector Laboratories, Burlingame, CA). Cell–substrate and cell–cell interactions were examined by scanning confocal microscopy on a stage maintained at 37 °C (live cell imaging). Imaging was performed on an LSM 700 scanning laser confocal microscope with an argon-ion laser (wavelengths 405, 488, 555, and 639 nm) fitted with a Zeiss 100 × PLAN Apochromat objective with a numerical aperture of 1.57 and with ZEN software (Carl Zeiss).

Assessment of Gene Expression in MSC Populations Using Fluidigm Biomark: In order to perform high-throughput quantitative genomics on 1 mm^2 electron-beam patterned samples, real-time qPCR was conducted using integrated microfluidic circuit analysis (Fluidigm Biomark HD system, UK). ≈600 hMSCs in 5 µL were seeded onto PDMS substrates at second passage (P2) and a cell density of 1.2 × 10^4 cells mL^{-1} for 12 h.

RNA Isolation: RNA was isolated from hMSCs using an ARCTURUS PicoPure RNA isolation kit according to manufacturer instructions (Applied Biosystems, UK). RNA quality and quantity was measured with 2100 Bioanalyser and RNA 6000 Pico Kit, again according to manufacturer's protocol (Agilent Technologies, USA). Samples with a RIN value > 7 was further processed for cDNA conversion. Briefly, total RNA (≈20 ng) was amplified with High Capacity RNA-to-cDNA Kit (Applied Biosystems) using MJ Research PTC 200 Thermal Cycler (Thermo Scientific, Ireland).

Fluidigm Genomic Analysis: The RNA was subjected to a reverse transcription using the SuperScript III Reverse Transcriptase (Invitrogen, UK). At all stages of the process, reactions were performed at 4 °C unless stated. Gene analysis was performed using the Fluidigm Fastgene expression Analysis using EvaGreen on the Biomark HD system protocol (PN 100-3488 C1). In brief, all 96 primers were pooled together (1 µL from each primer set pooled in 104 µL of DNA suspension buffer). Preamplification was prepared using 1.25 µL of the cDNA from each sample, 2.5 µL 2× Multiplex Master Mix (Qiagen), 0.5 µL pooled primer mix, and 0.75 µL water. This was vortexed, centrifuged, and subjected to 22 thermal cycles with the following programme:

Condition	Hold	18 cycles		Extension	Hold
Temperature	95 °C	94 °C	60 °C	72 °C	4 °C
Time	15 min	30 s	90 s	10 min	∞

After the 18 thermal cycles, 1.4 µL water, 0.2 µL exonuclease I reaction buffer, and 0.4 µL exonuclease were added to each sample and vortexed, centrifuged, and incubated at 37 °C for 30 min followed by 80 °C for 15 min. Following heat inactivation, 18 µL of TE buffer was added to each sample. 2.7 µL of the exonuclease I treated sample was added to 3.0 µL 2× SsoFast EvaGreen Supermix (Bio-Rad) and 0.3 µL 20× DNA binding dye sample loading reagent (Fluidigm). Each mixture was vortexed and centrifuged ready to be loaded onto the chip. Additionally, 0.3 µL of each individual primer set was added to 3 µL 2× assay loading reagent and 2.7 µL 1× DNA suspension buffer, vortexed and centrifuged ready for loading on the chip and run on the Fluidigm Biomark HD system. A 96.96 Dynamic array integrated fluidic circuit was used during this analysis.

Analysis of Signaling Pathways: A total of 87 target genes were probed and the gene targets were expressed as relative fold-change to the differentiation controls (Table S1, Supporting Information). IPA (Ingenuity Systems, Qiagen) was used to identify canonical signaling and functional pathways. The plots were normalized relative to the control samples on plain PDMS treated with chondrogenic media (Poietics PT-4124; Lonza, Walkersville, MD) or osteogenic media (Poietics PT-3924; Lonza, Walkersville, MD). Comparison analysis on differential gene expression between the samples was performed with a false discovery rate <0.05 (Fischer's exact test) and fold change >1.3.

Time-Lapse Videomicroscopy: Time-lapse studies were performed as described elsewhere.[52] Briefly, MSCs were seeded onto patterned and control PDMS substrata and incubated for 1 h to allow cells to adhere. Cell media as subsequently removed and cells cultured in CO_2 independent medium (Gibco) supplemented with 10% fetal bovine serum, 1% L-glutamine, and 100 IU mg^{-1} penicillin/streptomycin (Invitrogen). The substrates were sandwiched to an aluminum microscope slide with vacuum grease. Time-lapse microscopy images were recorded with a 20×, 0.7 NA air objective (Olympus) through a cooled CCD camera CoolSNAP HQ (Roper Scientific Inc.) using Simple PCI software (Compix Inc.). Images were captured via DIC microscopy every 5 min.

Image Analysis: All images were analyzed using ImageJ (National Institutes of Health). Image stacks consisted of 2–3 planes spaced by 0.40 µm, which were rendered using standard deviation image intensity to produce a single image of the ventral cell surface. Focal adhesions were analyzed in cells from three separate experiments (20 cells each). FA/exposed spot colocalization was analyzed by Mander's method with the JACoP plugin.[53] Mander's overlap coefficient is based on the Pearson's correlation coefficient with average intensity values being taken out of the mathematical expression.[54] This coefficient will vary from 0 to 1, the former corresponding to nonoverlapping images and the latter reflecting 100% colocalization between both images. Therefore, M1 (or M2) determined the proportion of the fluorescent paxillin signal coincident with the DIC signal of the substrate over its total intensity, given as the following: $k_1 = S_i(A_{i,\,coloc}))/(S_iA_i)$ and $k_2 = (S_i(B_{i,\,coloc}))/(S_iB_i)$ with $A_{i,\,coloc}$ being A_i if $B_i > 0$ and 0 if $B_i = 0$; and $B_{i,\,coloc}$ being B_i if $A_i > 0$ and 0 if $A_i = 0$. Live-cell analysis of cell motility was performed with the ImageJ plugin MTrackJ.[55]

Statistical Analysis: All statistical analysis was performed with SPSS Statistics software 20 (IBM, USA) unless otherwise noted. Data are expressed as mean ± SEM with * and ** indicating a 95% and 99.5% confidence interval, respectively. ANOVA was used to determine statistical significance followed by post hoc Bonferoni's multiple test correction to determine which groups were statistically different. A right-tailed Fisher's exact test was applied to identify significance in activation pathways extracted from individual changes at the genetic level through IPA analysis.

Supporting Information

Supporting Information is available from the Wiley Online Library or from the author.

Acknowledgements

M.B. is a Science Foundation Ireland fellow and was supported by Grant No. 11/SIRG/B2135. This work carried out by M.B., J.L., and S.W. was funded principally by the National Institutes of Health (NIH) Common Fund Nanomedicine program (PN2EY016586). The authors would like to thank Ms. Jessica Brann for microscopy support, Ms. Gemma Orpella for primer design, Mr. Geoff Goold for technical assistance, Prof. Michael Sheetz and Prof. Michael Dustin for their help, advice, and useful discussion, and Mr. Maciej Doczyk (http://doczykdesign.com) for graphic design.

Conflict of Interest

The authors declare no conflict of interest.

Keywords

electron beam, focal adhesions, mechanotransduction, polydimethylsiloxane, rigidity, stem cells

Received: April 15, 2017
Revised: July 3, 2017
Published online: September 1, 2017

[1] T. Pompe, S. Glorius, T. Bischoff, I. Uhlmann, M. Kaufmann, S. Brenner, C. Werner, *Biophys. J.* **2009**, *97*, 2154.
[2] B. N. Mason, J. P. Califano, C. A. Reinhart-King, *Eng. Biomater. Regener. Med.* **2012**, *2*, 19.
[3] G. Giannone, B. J. Dubin-Thaler, H. G. Dobereiner, N. Kieffer, A. R. Bresnick, M. P. Sheetz, *Cell* **2004**, *116*, 431.
[4] L. Trichet, J. Le Digabel, R. J. Hawkins, S. R. Vedula, M. Gupta, C. Ribrault, P. Hersen, R. Voituriez, B. Ladoux, *Proc. Natl. Acad. Sci. USA* **2012**, *109*, 6933.

[5] D. E. Discher, P. Janmey, Y. L. Wang, *Science* **2005**, *310*, 1139.
[6] V. Vogel, M. Sheetz, *Nat. Rev. Mol. Cell Biol.* **2006**, *7*, 265.
[7] A. J. Engler, S. Sen, H. L. Sweeney, D. E. Discher, *Cell* **2006**, *126*, 677.
[8] a) S. W. Moore, P. Roca-Cusachs, M. P. Sheetz, *Dev. Cell* **2010**, *19*, 194; b) K. L. Marshall, E. A. Lumpkin, *Adv. Exp. Med. Biol.* **2012**, *739*, 142.
[9] S. Ghassemi, G. Meacci, S. Liu, A. A. Gondarenko, A. Mathur, P. Roca-Cusachs, M. P. Sheetz, J. Hone, *Proc. Natl. Acad. Sci. USA* **2012**, *109*, 5328.
[10] T. Shemesh, B. Geiger, A. D. Bershadsky, M. M. Kozlov, *Proc. Natl. Acad. Sci. USA* **2005**, *102*, 12383.
[11] a) A. del Rio, R. Perez-Jimenez, R. Liu, P. Roca-Cusachs, J. M. Fernandez, M. P. Sheetz, *Science* **2009**, *323*, 638; b) P. Kanchanawong, G. Shtengel, A. M. Pasapera, E. B. Ramko, M. W. Davidson, H. F. Hess, C. M. Waterman, *Nature* **2010**, *468*, 580.
[12] a) M. J. Biggs, R. G. Richards, N. Gadegaard, C. D. Wilkinson, R. O. Oreffo, M. J. Dalby, *Biomaterials* **2009**, *30*, 5094; b) M. J. Biggs, R. G. Richards, M. J. Dalby, *Nanomedicine* **2010**, *6*, 619.
[13] D. Sanchez, N. Johnson, C. Li, P. Novak, J. Rheinlaender, Y. J. Zhang, U. Anand, P. Anand, J. Gorelik, G. I. Frolenkov, C. Benham, M. Lab, V. P. Ostanin, T. E. Schaffer, D. Klenerman, Y. E. Korchev, *Biophys. J.* **2008**, *95*, 3017.
[14] M. P. E. Wenger, L. Bozec, M. A. Horton, P. Mesquida, *Biophys. J.* **2007**, *93*, 1255.
[15] S. Saber-Samandari, K. A. Gross, *Acta Biomater.* **2009**, *5*, 2206.
[16] A. Crow, K. D. Webster, E. Hohlfeld, W. P. Ng, P. Geissler, D. A. Fletcher, *Biophys. J.* **2012**, *102*, 443.
[17] S. Moeinzadeh, S. R. P. Shariati, E. Jabbari, *Biomaterials* **2016**, *92*, 57.
[18] I. E. Palama, S. D'Amone, A. M. Coluccia, M. Biasiucci, G. Gigli, *Integr. Biol.* **2012**, *4*, 228.
[19] a) A. Tropmann, L. Tanguy, P. Koltay, R. Zengerle, L. Riegger, *Langmuir* **2012**, *28*, 8292; b) G. Lin, V. I. Wu, R. E. Hainley, L. A. Flanagan, E. S. Monuki, W. C. Tang, *Conf. Proc. IEEE Eng. Med. Biol. Soc.* **2004**, *4*, 2607.
[20] Y. Sun, L. T. Jiang, R. Okada, J. Fu, *Langmuir* **2012**, *28*, 10789.
[21] B. Trappmann, J. E. Gautrot, J. T. Connelly, D. G. Strange, Y. Li, M. L. Oyen, M. A. C. Stuart, H. Boehm, B. Li, V. Vogel, J. P. Spatz, F. M. Watt, W. T. Huck, *Nat. Mater.* **2012**, *11*, 642.
[22] Y. N. Xia, G. M. Whitesides, *Annu. Rev. Mater. Sci.* **1998**, *28*, 153.
[23] K. Tsougeni, A. Tserepi, E. Gogolides, *Microelectron. Eng.* **2007**, *84*, 1104.
[24] a) J. M. Desimone, G. A. York, J. E. Mcgrath, A. S. Gozdz, M. J. Bowden, *Macromolecules* **1991**, *24*, 5330; b) R. Giri, M. S. Sureshkumar, K. Naskar, Y. K. Bharadwaj, K. S. S. Sarma, S. Sabharwal, G. B. Nando, *Adv. Polym. Technol.* **2008**, *27*, 98.
[25] M. T. Russell, L. S. C. Pingree, M. C. Hersam, T. J. Marks, *Langmuir* **2006**, *22*, 6712.
[26] a) M. J. Paszek, N. Zahir, K. R. Johnson, J. N. Lakins, G. I. Rozenberg, A. Gefen, C. A. Reinhart-King, S. S. Margulies, M. Dembo, D. Boettiger, D. A. Hammer, V. M. Weaver, *Cancer Cell* **2005**, *8*, 241; b) J. Liu, Y. Tan, H. Zhang, Y. Zhang, P. Xu, J. Chen, Y. C. Poh, K. Tang, N. Wang, B. Huang, *Nat. Mater.* **2012**, *11*, 734.
[27] T. J. Young, M. A. Monclus, T. L. Burnett, W. R. Broughton, S. L. Ogin, P. A. Smith, *Meas. Sci. Technol.* **2011**, *22*, DOI: 10.1088/09570233/22/12/125703.
[28] D. K. Cai, A. Neyer, R. Kuckuk, H. M. Heise, *J. Mol. Struct.* **2010**, *976*, 274.
[29] L. Albers, J. Baumgartner, C. Marschner, T. Muller, *Chem. - Eur. J.* **2016**, *22*, 7970.
[30] B. Y. Liu, J. Fu, *J. Micromech. Microeng.* **2015**, *25*.
[31] J. Bowen, D. Cheneler, A. P. G. Robinson, *Microelectron. Eng.* **2012**, *97*, 34.
[32] a) S. L. Zhu, H. H. Cheng, I. Blakey, N. Stokes, K. Ostrikov, M. Cortie, *Microelectron. Eng.* **2015**, *139*, 13; b) J. R. Gamboa, S. Mohandes, P. L. Tran, M. J. Slepian, J. Y. Yoon, *Colloids Surf., B* **2013**, *104*, 318.
[33] M. J. Dalby, N. Gadegaard, R. Tare, A. Andar, M. O. Riehle, P. Herzyk, C. D. W. Wilkinson, R. O. C. Oreffo, *Nat. Mater.* **2007**, *6*, 997.
[34] B. Schnyder, T. Lippert, R. Kotz, A. Wokaun, V. M. Graubner, O. Nuyken, *Surf. Sci.* **2003**, *532*, 1067.
[35] C. Monge, N. Saha, T. Boudou, C. Pozos-Vasquez, V. Dulong, K. Glinel, C. Picart, *Adv. Funct. Mater.* **2013**, *23*, 3432.
[36] a) E. Cukierman, R. Pankov, D. R. Stevens, K. M. Yamada, *Science* **2001**, *294*, 1708; b) M. J. Biggs, R. G. Richards, N. Gadegaard, C. D. Wilkinson, M. J. Dalby, *J. Mater. Sci.: Mater. Med.* **2007**, *18*, 399.
[37] K. Kulangara, Y. Yang, J. Yang, K. W. Leong, *Biomaterials* **2012**, *33*, 4998.
[38] M. J. Dalby, N. Gadegaard, R. Tare, A. Andar, M. O. Riehle, P. Herzyk, C. D. Wilkinson, R. O. Oreffo, *Nat. Mater.* **2007**, *6*, 997.
[39] R. J. Pelham, Y. L. Wang, *Proc. Natl. Acad. Sci. USA* **1997**, *94*, 13661.
[40] A. Nicolas, A. Besser, S. A. Safran, *Biophys. J.* **2008**, *95*, 527.
[41] a) S. P. Massia, J. A. Hubbell, *J. Cell Biol.* **1991**, *114*, 1089; b) B. Geiger, J. P. Spatz, A. D. Bershadsky, *Nat. Rev. Mol. Cell Biol.* **2009**, *10*, 21.
[42] E. A. Cavalcanti-Adam, T. Volberg, A. Micoulet, H. Kessler, B. Geiger, J. P. Spatz, *Biophys. J.* **2007**, *92*, 2964.
[43] S. V. Plotnikov, A. M. Pasapera, B. Sabass, C. M. Waterman, *Cell* **2012**, *151*, 1513.
[44] M. Arnold, M. Schwieder, J. Blummel, E. A. Cavalcanti-Adam, M. Lopez-Garcia, H. Kessler, B. Geiger, J. P. Spatz, *Soft Matter* **2009**, *5*, 72.
[45] C. Yang, F. W. DelRio, H. Ma, A. R. Killaars, L. P. Basta, K. A. Kyburz, K. S. Anseth, *Proc. Natl. Acad. Sci. USA* **2016**, *113*, E4439.
[46] I. T. Hoffecker, W. H. Guo, Y. L. Wang, *Lab Chip* **2011**, *11*, 3538.
[47] G. Meacci, M. Stachowiak, S. M. Liu, T. Iskratsch, A. Mathur, H. Wolfenson, S. Ghassemi, P. Roca-Cusachs, E. Tabdanov, N. Gauthier, A. Gondarenko, B. O'Shaughnessy, J. Hone, M. Sheetz, *Biophys. J.* **2013**, *104*, 477A.
[48] A. O'Reilly, D. J. Kelly, *Ann. Biomed. Eng.* **2016**, *44*, 3446.
[49] a) L. Gao, R. McBeath, C. S. Chen, *Stem Cells* **2010**, *28*, 564; b) A. Woods, G. Y. Wang, F. Beier, *J. Biol. Chem.* **2005**, *280*, 11626.
[50] Monte Carlo simulation of electron trajectory in solids - CASINO, http://www.gel.usherbrooke.ca/casino/ (accessed: Aug 2017).
[51] D. Thomas, G. Fontana, X. Z. Chen, C. Sanz-Nogues, D. I. Zeugolis, P. Dockery, T. O'Brien, A. Pandit, *Biomaterials* **2014**, *35*, 8757.
[52] M. J. Biggs, M. C. Milone, L. C. Santos, A. Gondarenko, S. J. Wind, *J. R. Soc. Interface* **2011**, *8*, 1462.
[53] S. Bolte, F. P. Cordelieres, *J. Microsc.* **2006**, *224*, 213.
[54] K. W. Dunn, M. M. Kamocka, J. H. McDonald, *Am. J. Physiol.* **2011**, *300*, C723.
[55] E. Meijering, O. Dzyubachyk, I. Smal, *Methods Enzymol.* **2012**, *504*, 183.

